

# **Starlight Suppression: Technologies for Direct Imaging of Exoplanets**

Dmitry Savransky

Sibley School of Mechanical and Aerospace Engineering

Cornell University, Ithaca, NY 14853, USA

8/3/2015

Of the nearly two thousand planets confirmed to exist outside of the solar system, only a small handful were detected directly rather than inferred from their interaction with their host stars. The vast majority of known exoplanets were discovered by sifting years of observations of thousands of stars for periodic changes in the stars' colors or fluxes, which indicate an orbiting planet. Imaging, on the other hand, allows for detection with just one observation, and confirmation with a few observations taken only months apart. More importantly, imaging exoplanets allows us to spectroscopically characterize them, often at spectral resolutions significantly exceeding what is possible with any other detection method. Spectroscopy allows us to probe the atmospheric, and potentially surface, composition of exoplanets and validate models of planet formation and evolution.

Imaging is therefore a crucial component of our exoplanet detection and characterization toolbox. Exoplanet imagers on ground observatories are already producing exciting discoveries and the next generation of space instrumentation has the potential to detect Earth-like planets, and find indications of the presence of life. This short paper reviews the fundamental challenges in imaging exoplanets, along with the techniques used to overcome them and the status of current technology development for exoplanet imagers in space.

# 1 Imaging of Exoplanets

A telescope operates by collecting light from an astronomical source using a finite-sized aperture—either the entrance pupil of a refractive system or the primary mirror of a reflective one—and bringing the light to a focus on an imaging detector, such as a charge-coupled device (CCD). Diffraction effects limit the spatial resolving capabilities of telescopes, with angular resolution inversely proportional to the size of the aperture. For a circular pupil the minimum angular resolution ( $\alpha_r$ ) of the system will be greater than approximately  $1.22\lambda/D$  where  $\lambda$  is the wavelength of light and  $D$  the diameter of the aperture. This is most easily understood by considering the point spread function (PSF) of the telescope—the impulse response generated by imaging a point source. For a circular aperture, the PSF is an Airy disk, shown in Figure 1—a bright central spot of radius  $\alpha_r$ , surrounded by a series of annuli that decrease exponentially in brightness with angular separation. Between these annuli are small, dark regions called nulls.

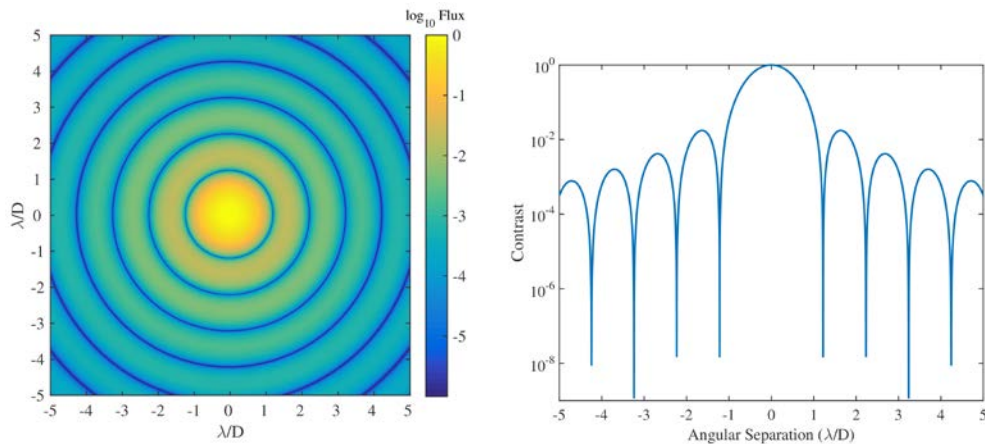
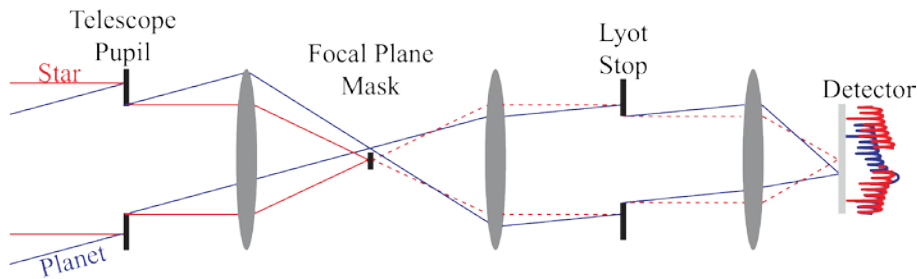


Figure 1: Numerical simulation of an Airy disk—the impulse response of a circular aperture. Left: Image of a point source, with color indicating intensity in log scale. Right: The (radially symmetric) contrast profile of the image.

Planets are significantly fainter than their host stars, with contrasts of  $10^6$  for the very brightest, self-luminous, young, Jovian planets, and  $10^{10}$  for Earth-sized planets in reflected, visible light. Assuming that we happened to catch a planet when it was precisely located on one of the deeper nulls of a perfect, diffraction-limited telescope, we still would not be able to image it, as no detector has the dynamic range required to capture both signals from the planet as well as the PSF of the star in the same image.

## 2 Coronagraphy

Fortunately, this problem was partially solved in the early 20th century by solar astronomers studying the sun’s corona, which is one million times fainter than the sun itself. Previously, the corona could only be studied during full solar eclipses. In the 1930s, however, Bernard Lyot demonstrated the first solar coronagraph—a system design specifically to block bright, on-axis sources, to allow for the study of faint, off-axis ones (Lyot, 1939).



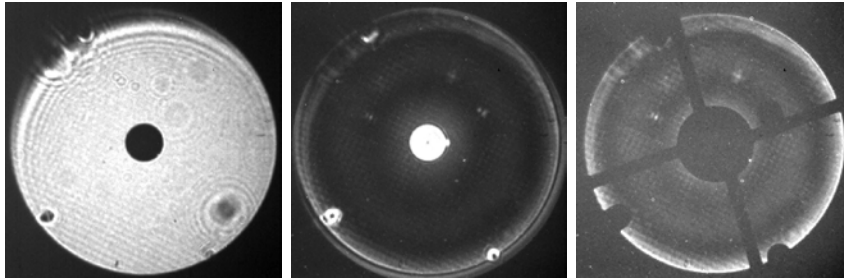


Figure 2: Top: Schematic of a Lyot coronagraph. Based on Sivaramakrishnan et al. (2001). Bottom: Images taken at the pupil plane of the Lyot stop showing (left) the unobscured entrance pupil, (middle) only the focal plane mask, and (right) both the focal plane mask and Lyot stop. Each image is individually stretched and the final image has less than 1% of the light in the first image.

Figure 2 shows a schematic view of a Lyot coronagraph, along with images taken at a pupil of a coronagraphic system. This pupil is conjugate with the entrance pupil of the whole system, so that the first image, where no coronagraph elements are in place, is equivalent to the intensity distribution seen by the entrance aperture of the whole system. The central dark spot in the first image is due to the secondary mirror that partially obscures the primary aperture in this system. On-axis starlight, along with off-axis planet light enters the telescope and is brought to a focus, where the on-axis source is blocked by a small, hard-edged focal plane mask (FPM). The remaining light is propagated to the next pupil plane, as in the second image. While most of the starlight is blocked by the FPM, some will diffract around the mask's edges, creating a pattern of rings along with a bright central spot. These are blocked by introducing another hard edged mask, called a Lyot stop, into the pupil leaving very little residual light, as in the third image. The Lyot stop can also include additional features to handle diffraction about other mechanical elements, such as struts that hold up the secondary mirror.

To deal with residual diffracted light in the classical Lyot coronagraph, an additional pupil plane can be introduced before the FPM with a partially transmissive mask to apodize the beam so that diffraction effects downstream are minimized (Soummer, 2005). An alternate approach is to introduce a specially shaped hard-edged pupil ahead of the FPM to change the PSF so it is no longer radially symmetric, leaving high contrast regions in the downstream focal plane (Kasdin et al., 2005). Other strategies involve replacing the hard-edged FPM of the original Lyot coronagraph with a phase-shift mask in order to produce destructive interference of the on-axis light (Roddier and Roddier, 1997). One can also achieve the beam apodization by using pupil-mapping mirrors to change the geometrical redistribution of the light (Guyon et al., 2005).

All of these approaches have various pros and cons, but all share the same basic limitations. Coronagraphs are still limited by the diffraction limit of the telescope, and most designs remove part of the planet light as well as the starlight. A particular coronagraph's design is highly specific to a particular telescope design. Finally, many coronagraph designs are highly sensitive to misalignment, vibration, and optical surface errors. Coronagraphs being evaluated for use in space all rely on introducing active wavefront control via deformable mirrors, which have only recently begun to be demonstrated for use in space (Cahoy et al., 2014).

### **3 Starshades**

An alternate approach, first suggested by Spitzer (1962), involves blocking the starlight before it ever enters the telescope. This method requires a space telescope to fly in formation, over a baseline of tens of thousands of kilometers, with an occulting spacecraft, or starshade. The starshade must be tens of meters in diameter and specifically shaped, as diffraction effects would

cause light to be scattered back into the shadow cast by a simple flat plate. Fortunately, by Babinet's principle, the occulter becomes complementary to a pinhole camera, allowing starshades to be designed in much the same way as shaped pupil masks for internal coronagraphs, via numerical optimization (Vanderbei et al., 2007). This allows for constraints to be placed on minimum feature sizes to ensure that the produced designs are manufacturable. The resulting optimized shapes are radially symmetric, with a circular central core surrounded by petal-like extensions, as in Figure 3.

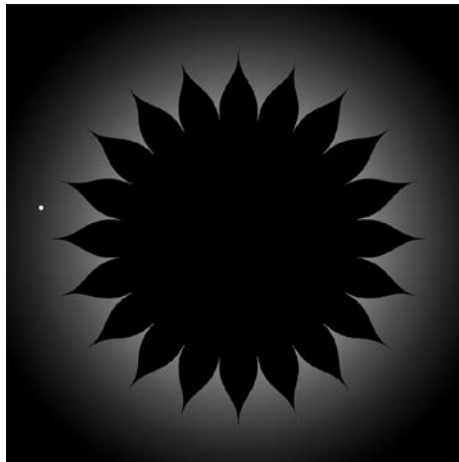


Figure 3: Schematic view of a starshade as seen by an occulted telescope. The starshade creates a shadow region of high contrast at the telescope aperture, allowing for exoplanets to be detected. Based on Vanderbei et al. (2007).

The main advantage of starshades is that they can achieve high contrasts with any conventional telescope design and without any active wavefront control. Furthermore, the minimum angular separation of a detectable planet for a starshade is determined solely by geometry—the size of the starshade and its distance from the telescope—and is the same at all

wavelengths. On the other hand, while a telescope with an internal coronagraph merely needs to pivot in order to observe a new target, a starshade must be repositioned over large distances, with weeks of slew time in between observations, leading to fewer stars observed and making scheduling optimization more difficult (Savransky et al., 2010). Starshade contrasts are also highly sensitive to shape, positioning and alignment errors, leading to  $\mu\text{m}$  order manufacturing tolerances, mm deployment tolerances, and meter-scale alignment tolerances held throughout the course of an observation (Shaklan et al., 2010). The requirement for precise alignment for extended periods also makes the formation flying problem more difficult in geocentric orbits, so that most starshade mission concepts assume operations about the second Earth-Sun Lagrange point (Kolemen et al., 2012). Finally, unlike coronagraphs, it is impossible to fully test starshades on the ground, so that proxy experiments must be constructed to build confidence in this technique (Sirbu et al., 2014).

## **4 Current and Future Exoplanet Imagers**

Multiple exoplanet imagers, including the Gemini Planet Imager (Macintosh et al., 2014) and SPHERE (Savane et al., 2013) are currently operating at some of the largest ground-based observatories. These instruments couple advanced coronagraphs with extreme adaptive optics systems (Tyson, 2010), which correct for the effects of the turbulent atmosphere, to produce the highest levels of contrast ever demonstrated from the ground. Still, these systems will only be able to detect the very youngest, self-luminous giant planets on relatively large orbits—akin to Jupiter in the first 100 million years of its existence. Advances in adaptive optics and coronagraphy, and the construction of the next generation of extremely large telescopes will

allow for the detection of smaller, older planets, but our best chance of directly imaging and getting spectra of an Earth-like planet lies in space.

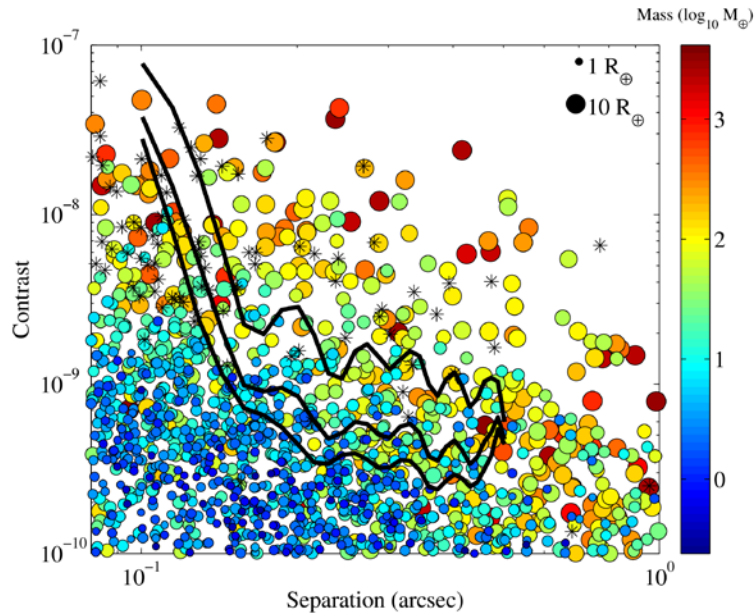


Figure 4: Colored points represent a simulated population of exoplanets based on prior surveys, star markers represent contrast estimates for known, indirectly detected exoplanets at their most favorable viewing geometries, and the black curves are the predicted contrasts for one design of the WFIRST coronagraph at various levels of telescope stability. Based on Savransky (2013).

Currently, NASA is developing a coronagraphic instrument for the Wide Field Infrared Space Telescope (WFIRST; Spergel et al., 2015), the next major astrophysics mission to be launched after the James Webb Space Telescope. The WFIRST coronagraph will be capable of detecting a wide variety of exoplanets, including planets like Neptune, as well super-Earths—a class of potentially rocky planets up to twice the radius of the Earth, which do not exist in our

own solar system. Figure 4 shows a simulation of the population of planets around nearby stars, based on statistics from indirect surveys (Fressin et al., 2013; Howard et al., 2010), along with the expected contrast of one design for the WFIRST coronagraph with varying assumptions of telescope stability (Krist, 2014). The NASA Astrophysics Division has also sponsored two Science and Technology Definition Teams to study \$1B class mission concepts based on a starshade (Exo-S) and coronagraph (Exo-C). These and other concept studies are helping identify the remaining engineering challenges in direct imaging, and guiding technology development programs. Thanks to these efforts, we may have a space-based direct imaging instrument operating within the next decade, producing exciting new science and helping validate the technologies needed to discover Earth-like planets and potentially find alien life.

For more information on WFIRST, see <http://wfirst.gsfc.nasa.gov/> and for more information on Exo-S and Exo-C, see <https://exep.jpl.nasa.gov/stdt/>.

## References

Kerri L Cahoy, Anne D Marinan, Benjamin Novak, Caitlin Kerr, Tam Nguyen, Matthew Webber, Grant Falkenburg, and Andrew Barg. Wavefront control in space with mems deformable mirrors for exoplanet direct imaging. *Journal of Micro/Nanolithography, MEMS, and MOEMS*, 13 (1): 011105–011105, 2014.

François Fressin, Guillermo Torres, David Charbonneau, Stephen T Bryson, Jessie Christiansen, Courtney D Dressing, Jon M Jenkins, Lucianne M Walkowicz, and Natalie M Batalha. The false positive rate of kepler and the occurrence of planets. *The Astrophysical Journal*, 766 (2): 81, 2013.

Olivier Guyon, Eugene A Pluzhnik, Raphael Galicher, Frantz Martinache, Stephen T Ridgway, and Robert A Woodruff. Exoplanet imaging with a phase-induced amplitude apodization coronagraph. I. Principle. *The Astrophysical Journal*, 622 (1): 744, 2005.

A.W. Howard, G.W. Marcy, J.A. Johnson, D.A. Fischer, J.T. Wright, H. Isaacson, J.A. Valenti, J. Anderson, D.N.C. Lin, and S. Ida. The occurrence and mass distribution of close-in super-earths, neptunes, and jupiters. *Science*, 330 (6004): 653–655, 2010.

N. J. Kasdin, R. J. Vanderbei, M. G. Littman, and D. N. Spergel. Optimal one-dimensional apodizations and shaped pupils for planet finding coronagraphy. *Applied optics*, 44 (7): 1117–1128, 2005.

Egemen Kolemen, N Jeremy Kasdin, and Pini Gurfil. Multiple poincaré sections method for finding the quasiperiodic orbits of the restricted three body problem. *Celestial Mechanics and Dynamical Astronomy*, 112 (1): 47–74, 2012.

John E Krist. End-to-end numerical modeling of AFTA coronagraphs. In *SPIE Astronomical Telescopes+ Instrumentation*, pages 91430V–91430V. International Society for Optics and Photonics, 2014.

Bernard Lyot. The study of the solar corona and prominences without eclipses (George Darwin Lecture, 1939). *Monthly Notices of the Royal Astronomical Society*, 99: 580, 1939.

Bruce Macintosh, James R. Graham, Patrick Ingraham, Quinn Konopacky, Christian Marois, Marshall Perrin, Lisa Poyneer, Brian Bauman, Travis Barman, Adam S. Burrows, Andrew Cardwell, Jeffrey Chilcote, Robert J. De Rosa, Daren Dillon, Rene Doyon, Jennifer Dunn, Darren Erikson, Michael P. Fitzgerald, Donald Gavel, Stephen Goodsell, Markus Hartung, Pascale Hibon, Paul Kalas, James Larkin, Jerome Maire, Franck Marchis, Mark S. Marley, James McBride, Max Millar-Blanchaer, Katie Morzinski, Andrew Norton, B. R. Oppenheimer, David Palmer, Jennifer Patience, Laurent Pueyo, Fredrik Rantakyro, Naru Sadakuni, Leslie Saddlemyer, Dmitry Savransky, Andrew

Serio, Remi Soummer, Anand Sivaramakrishnan, Inseok Song, Sandrine Thomas, J. Kent Wallace, Sloane Wiktorowicz, and Schuyler Wolff. First light of the Gemini Planet Imager. *Proceedings of the National Academy of Sciences*, 111 (35): 12661–12666, 2014. 10.1073/pnas.1304215111.

François Roddier and Claude Roddier. Stellar coronagraph with phase mask. *Publications of the Astronomical Society of the Pacific*, pages 815–820, 1997.

Jean-François Sauvage, Jean-Luc Beuzit, Ronald Roelfsema, Markus Feldt, Kjetil Dohlen, David Mouillet, Pascal Puget, Francois Wildi, Lyu Abe, Andrea Baruffolo, et al. Sphere: complete laboratory performance and prediction for on-sky first light. In *SPIE Optical Engineering+Applications*, pages 88640B–88640B. International Society for Optics and Photonics, 2013.

D. Savransky, N. J. Kasdin, and E. Cady. Analyzing the designs of planet finding missions. *Publications of the Astronomical Society of the Pacific*, 122 (890): 401–419, April 2010.

Dmitry Savransky. Space mission design for exoplanet imaging. In *Proc. SPIE*, volume 8864 of *SPIE Optical Engineering+Applications*, pages 886403–886403. International Society for Optics and Photonics, 2013.

S. B. Shaklan, M. C. Noecker, A. S. Lo, T. Glassman, P. J. Dumont, E. O. Jordan, N. J. Kasdin, Jr. W. C. Cash, E. J. Cady, and P. R. Lawson. Error budgeting and tolerancing of starshades for exoplanet detection. In *Proceedings of SPIE*, volume 7731, 2010.

Dan Sirbu, N Jeremy Kasdin, and Robert J Vanderbei. Diffractive analysis of limits of an occulter experiment. In *SPIE Astronomical Telescopes+Instrumentation*, pages 91432P–91432P. International Society for Optics and Photonics, 2014.

Anand Sivaramakrishnan, Christopher D Koresko, Russell B Makidon, Thomas Berkefeld, and Marc J Kuchner. Ground-based coronagraphy with high-order adaptive optics. *The Astrophysical Journal*, 552 (1): 397, 2001.

R. Soummer. Apodized pupil lyot coronagraphs for arbitrary telescope apertures. *The Astrophysical Journal Letters*, 618 (2): L161–L164, 2005.

D Spergel, N Gehrels, C Baltay, D Bennett, J Breckinridge, M Donahue, A Dressler, BS Gaudi, T Greene, O Guyon, et al. Wide-field infrared survey telescope-astrophysics focused telescope assets wfirst-afta 2015 report. *arXiv preprint arXiv:1503.03757*, 2015.

Lyman Spitzer. The beginnings and future of space astronomy. *American Scientist*, pages 473–484, 1962.

Robert Tyson. *Principles of adaptive optics*. CRC press, 2010.

R. J. Vanderbei, E. Cady, and N. J. Kasdin. Optimal Occulter Design for Finding Extrasolar Planets. *The Astrophysical Journal*, 665 (1): 794–798, 2007.